



The change of rock mass pressure of Lianchengshan tunnel

Jianxun Chen¹ · Yanbin Luo¹ · Yao Li¹ · Pengyu Zhao¹ · Dao Xu² · Qingsong Wang¹

Received: 26 March 2019 / Accepted: 25 February 2020 / Published online: 20 April 2020
© Springer-Verlag GmbH Germany, part of Springer Nature 2020

Abstract

Based on Lianchengshan tunnel, the changing of rock mass pressure with deformation, time and distance from the excavation face is analyzed by means of field monitoring and numerical simulation, and the main conclusions are as follows: (1) When the deformation increases rapidly, the rock mass pressure decreases first and then increases. After the settlement and clearance convergence are stable, the pressure of rock mass in each part is still increasing slowly. (2) The rock mass pressure is mostly between 0.1 and 0.3 MPa, and the variation lasts about 65 to 70 days. (3) During the period from mid-bench construction to inverted arch construction, the variation ratio of rock mass pressure is very high, which indicates that the stabilization time of this stage is too long. Therefore, it is suggested to shorten the length of mid-bench and lower-bench appropriately. (4) The space influence range of the excavation face propulsion is about 2.5 times the tunnel diameter of the hole (42 m). To decrease the rock mass pressure, ring closure should be reached as soon as possible. It is recommended to speed up the construction of middle bench and lower bench.

Keywords Tunnel engineering · Soft rock · Rock mass pressure · Evolution process · Numerical simulation

Introduction

There are many serious disasters during the construction of tunnels in soft and weak rock, such as large deformation of initial support, shotcrete cracking and spalling, steel frame twisting and damage, cracking and spalling of the secondary linings (Miwa and Ogasawara 2005; Hou et al. 2015; John 1976; Borca 2002; Kimura et al. 1987; Dai et al. 2015; Zou et al. 2010; Liu et al. 2011; Chen et al. 2020). These disasters are closely related to changing rock mass pressure around a tunnel. Compared with the rock mass with good integrity, less joints and fissures, high strength and hardness. The rock mass pressure adjustment time of the soft and weak rock mass is longer and more complex (Guan and Zhao 2011). Therefore, it is important to analyze the evolution of the rock mass pressure in the soft and weak rock tunnel, which is important to ensure the safety and stability of tunnel structure.

In recent years, many researchers have studied the mechanical evolution of tunnel in soft and weak rock mass

by analytical calculation (Lai et al. 2016; Kontogianni et al. 2006; Wang 2014; Litwiniszyn 1956; Zuo et al. 2016; Hu and Huang 2001), numerical simulation (Shan 2016; Xu et al. 2017; Galli et al. 2004; Hwang et al. 2006; Shalabi 2005; Ng et al. 2004; Tang et al. 2000), laboratory model test (Lei et al. 2015; Yang et al. 2016; Meda et al. 2016; Lai et al. 2018), and in situ monitoring (Li 2012; Yu 2004; Qiu et al. 2018). Based on the analysis of the time–space effect of Wushaoling tunnel construction, it is reported that the rock mass pressure and deformation are restrained longitudinally by the excavation face. The influence range is about 1D in front of the tunnel excavation face and 2D behind the face. Within this space range, the rock mass pressure gradually releases with the increase of the distance from the working face, and the deformation gradually increases with the increase of the distance from the working face. Li et al. (2007) simulated the construction of a subway tunnel in Shenzhen using three-dimensional numerical simulation. It was found that the excavation of the tunnel had an influence on the surface settlement within the area with 1.5 times of tunnel diameter from excavation face. The changing rate of rock mass pressure at the excavation face was the fastest, and it reached stable after the supporting structure was completed when supporting structure was in the form of a full circle or oval. Liu (2007) summarized the

✉ Pengyu Zhao
ZPY19890303@163.com

¹ Chang'an University, Xi'an, China

² Guiyang Engineering Corporation Limited, Guiyang, China

variation characteristics of the rock mass pressure based on the monitoring data of Gonghe tunnel. It was found that the vertical stress of the rock mass increases with the increase of buried depth of deep-buried large-section tunnel. Yang et al. (2010) monitored the rock mass pressure during the underground excavation under high in-situ stress. The results showed that the rock mass pressure changing process could be divided into three stages: stress release, stress adjustment and stress stabilization. Zhao and Li (2012) carried out lab model test based on the Liangshui tunnel of Lanzhou–Chongqing railway. The changing process of the rock mass pressure was analyzed and summarized under three conditions of tunnel excavation, which included full section excavation with or without support, and bench excavation method with support. It was concluded that the application of support effectively optimizes the tunnel rock mass load release process during construction. Yang et al. (2016) carried out a physical model test of dynamic construction mechanics, and obtains the stress-time response curve of rock mass under the condition of tunnel excavation and lining support. According to the response curve, the mechanical response and behavior of rock mass in the construction process are analyzed, and the development trend of response curve is divided into five stages according to excavation and support. The excavation process is divided into five stages: zero growth stage, micro-growth stage, sharp decline stage, slow decrease stage and relatively stable stage; and the support process is divided into rapid growth stage and slow growth stage. In addition, through the analysis of different distance measurement points between the vertical line and the horizontal waist line of the tunnel and the edge of the tunnel, it shows that with the increase of the distance, the stress release amount of rock mass caused by tunnel excavation decreases, the release rate slows down, the sensitivity of mechanical response decreases, and the influence of lining support on the mechanical characteristics of rock mass

gradually weakens. Sun and Shang (2008) reported the relationship between space–time effect of rock mass deformation and collapse accident through investigation and statistics of 76 tunnel cases. The results show that more than 80% of the landslides occur in the sharp deformation section, 13% in the stable deformation section, and only about 7% in the rheological section. Yan et al. (2017) found that the rock mass pressure had a tendency to increase, fluctuate, and stabilize, the maximum value is located at the upper and middle bench by monitored the rock mass pressure of the Queershan tunnel.

It can be seen that most researches focus on the variation law of rock mass pressure with respect to construction time and distance to tunnel face. However, few researchers studied the rock mass pressure with the deformation. Moreover, many researches only used the single method of numerical simulation (Shan 2016; Xu et al. 2017; Galli et al. 2004; Hwang et al. 2006; Shalabi 2005) or theoretical calculation (Zuo et al. 2016; Hu and Huang 2001) in their studies, and neglected the importance of in-situ monitoring. In this study, in-situ monitoring and numerical simulation methods are used to study the evolution process of rock mass pressure at Lianchengshan expressway tunnel. The evolution law of rock mass pressure with respect to deformation, time and distance from the tunnel face are studied, which could provide reference for similar projects.

Project overview

Lianchengshan highway tunnel is located in Hanzhong City, Shaanxi Province. The location of Lianchengshan Highway Tunnel is shown in Fig. 1. It is a two-traffic three-lane two-tunnel project with the design speed of 80 km/h, a total length of 5794 m for the left line and 5812 m for the right line of the tunnel project. Except for the construction

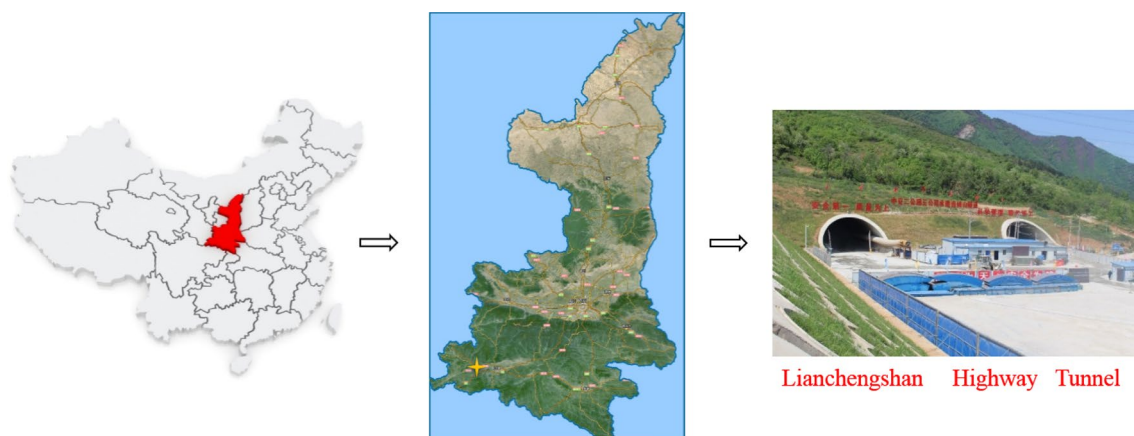


Fig. 1 Location of Lianchengshan Highway Tunnel

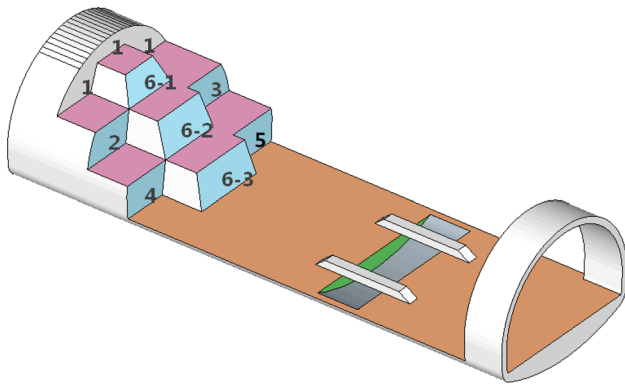


Fig. 2 Construction steps of Lianchengshan Tunnel

of Cross Center Diaphragms (CRD) method in gallery tunnel section and several sections with large deformation, Lianchengshan tunnel was constructed by three-bench and seven-step excavation method. The construction steps are shown in Fig. 2.

There were 12 stress-monitoring sections in the in situ monitoring (Fig. 6). In this paper, the ZK197 + 129 section was analyzed as a typical section for its best continuity of monitoring data and longer monitoring time. The project is located in the south of Qinling Mountains, with large topographic relief, steep valley slope and ridge. The geomorphic feature is mainly Zhongshan landform. According to the geomorphic genetic type, it can be divided into structural erosion accumulation landform and erosion structure landform. The results of hydraulic fracturing in-situ stress measurement show that the maximum horizontal principal stress (SH) is 20–21 MPa, the minimum horizontal principal stress (Sh) is 12–13 MPa. In addition, based on estimation of overlying rock mass volume-weight, the vertical principal stress (Sv) is 12–13 MPa. The minimum horizontal principal stress is slightly greater than the vertical principal stress, so the maximum horizontal principal stress is the maximum principal stress ($SH > Sh \geq Sv$). The buried depth of the tunnel is more than 250 m. The rock mass of excavation face is mainly chlorite mica schist, it is affected by the geological structure, and the integrity of the rock mass is very poor, mainly in the form of fragmentation, medium thick layer or thin layer. The dip direction of the rock layer is $320\text{--}350^\circ$ and the dip angle is $40^\circ\text{--}45^\circ$. The main minerals are chlorite, plagioclase, calcite, biotite and talc. The joints and folds of the rock mass are very developed, and there are many quartz veins or groundwater in some parts. The rock mass in some sections is broken into small pieces and schistose. The rock mass is loose, low strength in wet state, and disintegrated when encountering water. The ability of weathering resistance and self-stability of rock is very poor, and rock mass is easy to collapse along foliation tendency.

In situ test results show that the Poisson ratio of rock mass is 0.35, elastic modulus is 29.9 MPa, cohesion is 146.8 kPa, and friction angle is 32.5° . Based on the comprehensive analysis of in-situ stress conditions, mechanical parameters of rock mass and in-situ large deformation disaster, the expert group considers that the rock mass belongs to typical high ground stress soft rock.

The rock mass of excavation face is shown in Fig. 3. The supporting parameters are shown in Fig. 4.

Monitoring measurement scheme

The monitoring contents and methods of the Lianchengshan tunnel selected according to the requirement of “Technical Guidelines for Construction of Highway Tunnel” (Ministry of Communications of the People’s Republic of China, 2009) with emphase on stress monitoring for research. The instruments and sensors used in each monitoring section are shown in Table 1. Measured points for deformation monitoring are shown in Fig. 5. The layout and number of the monitoring points for initial supporting are shown in Fig. 6. In the monitoring of tunnel deformation, the non-contact method was used to avoid data missing and improve the measurement accuracy (Luo et al. 2016, 2017). Clearance convergence is used to describe the horizontal movement at

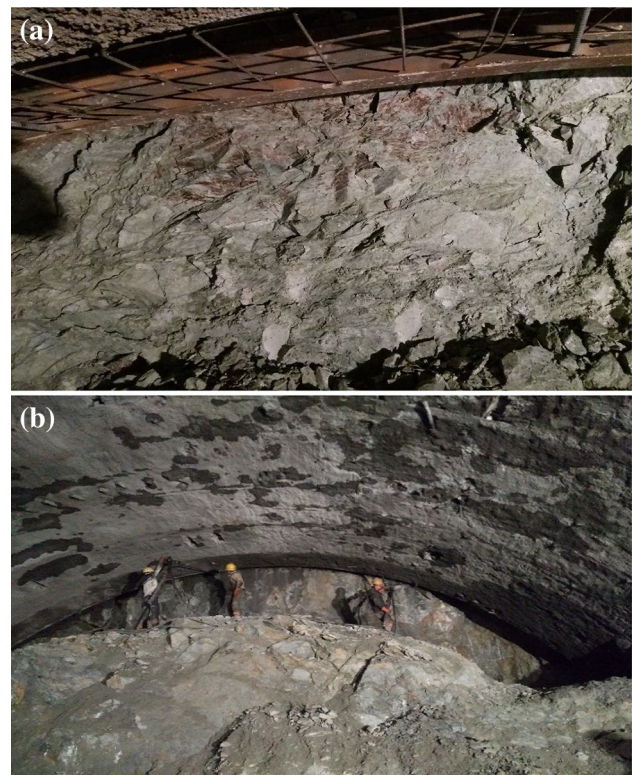


Fig. 3 Rock mass at excavation face

Fig. 4 Supporting parameters of Lianchengshan tunnel

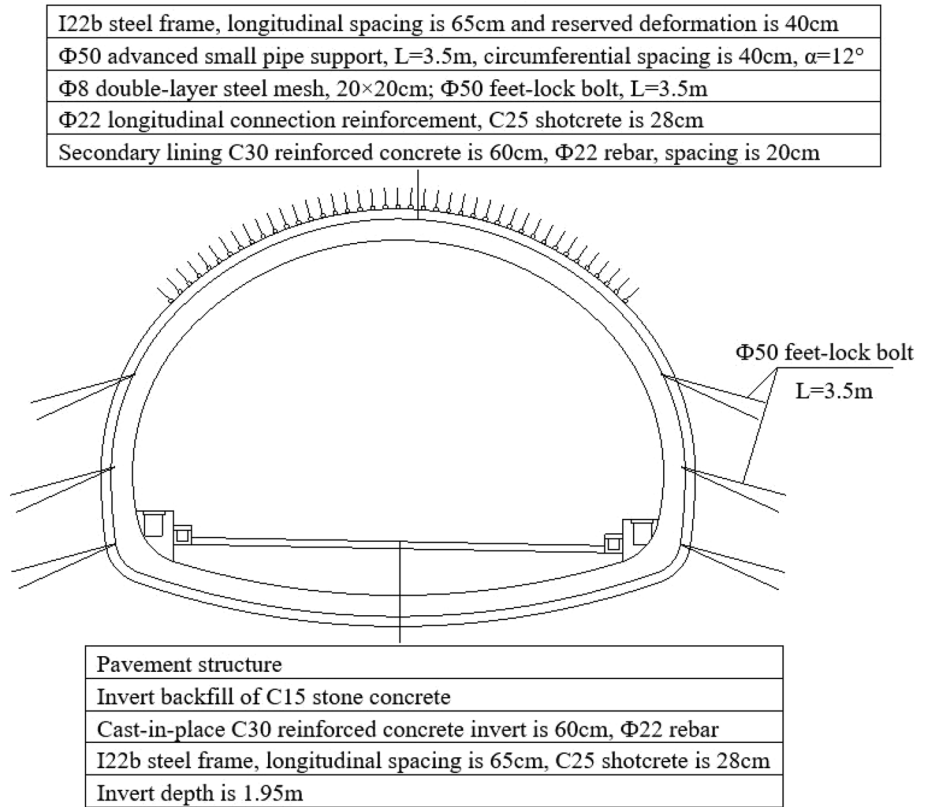


Table 1 Project and method of on-site monitoring measurement in Lianchengshan tunnel

Number	Monitor content	Instrument	Frequency	
1	Clearance convergence	TOPCON(OS-600G) Total station	1–15 days	1–2 times/day
			16 days-1 month	1 time/day
			After 1 month	1–2 times/week
2	Arch settlement	TOPCON(OS-600G) Total station	1–15 days	1–2 times/day
			16 days-1 month	1 time/day
			After 1 month	1–2 times/week
3	Rock mass pressure	Vibration string soil pressure box (0.5 MPa)	1 time/day	

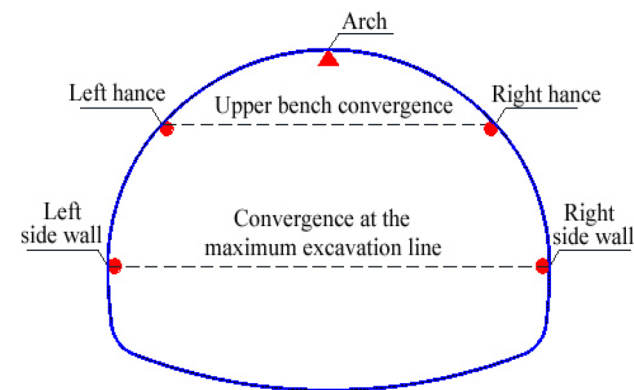


Fig. 5 Arrangement of deformation monitoring points and lines in monitoring section

the maximum excavation line which located in the horizontal direction with a maximum width. Arch settlement is used to describe the vertical movement at the crown.

Analysis of monitoring result

Change of rock mass pressure and deformation with time

The change of rock mass pressure and settlement with time are shown in Figs. 7 and 8 in which values measure from point 5 and 6 are presented as an example. In following figures, the number after Y corresponds to the number in

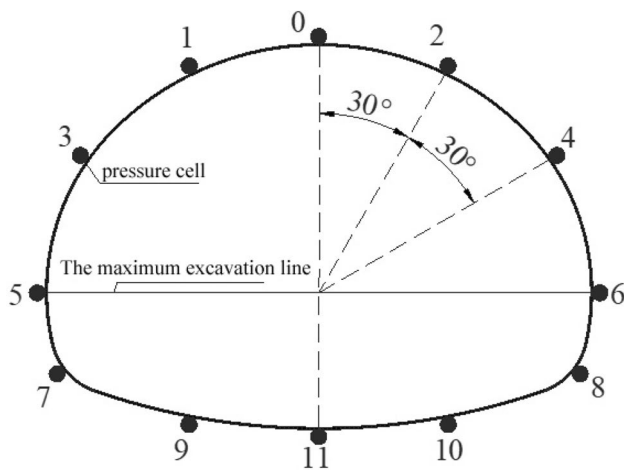


Fig. 6 Arrangement of soil pressure cells in monitoring section

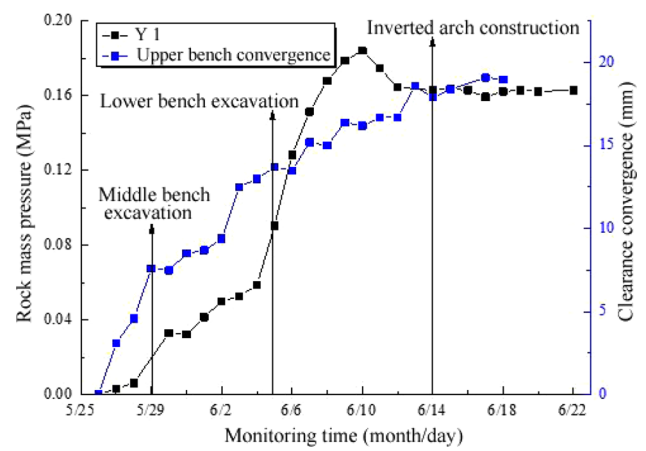


Fig. 9 Arch load and upper bench clearance convergence curve

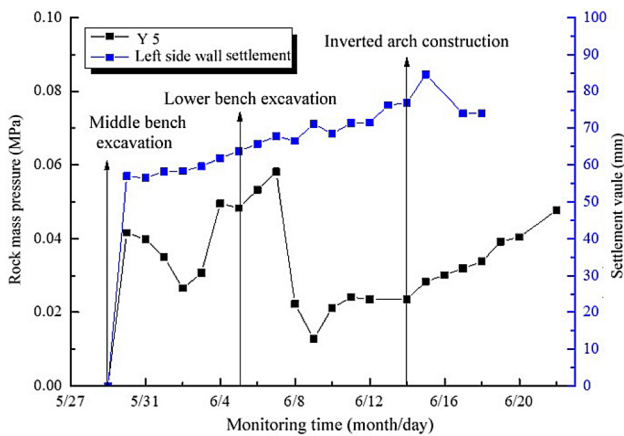


Fig. 7 Curve of rock mass pressure and settlement at point 5

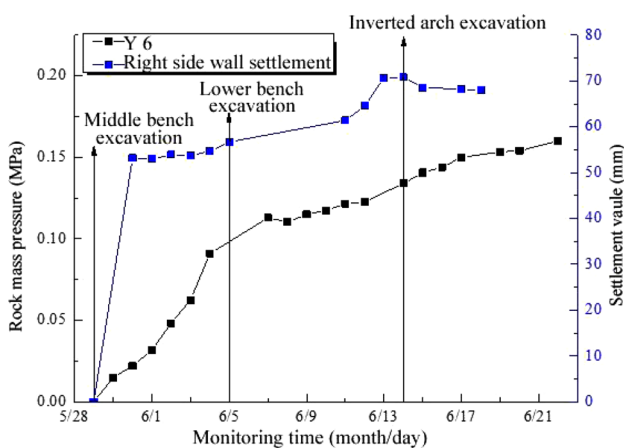


Fig. 8 Curve of rock mass pressure and settlement at point 6

Fig. 6, which is used to indicate the location of the measured point.

According to Figs. 7 and 8, it can be seen that the changing rock mass pressure with time has a similar trend with the changing settlement with time in general, but there is no significant correlation between them. At point 5, due to the loose contact of rock mass and supporting structure caused by excavation, there is some drop of rock mass pressure which leads to a complex relation between rock mass pressure and time. After further compaction of the loose rock mass, rock mass pressure increases. At point 6, rock mass pressure and settlement increased dramatically after the excavation of middle bench, and then maintained a relative stable state. It is interesting to note that settlement increases faster and reached a relative stable state within 3 days, while rock mass pressure increases slower compared with settlement and reached a relative stable state after 10 days. It indicated that the supporting structure can effectively control the settlement, and maintained a relative stable state when rock mass pressure increases.

The change of rock mass pressure and convergence with time are shown in Figs. 9 and 10 in which values measure from point 1, 5 and 6 are presented as an example. In Fig. 9, settlement increases gradually in the first 15 days, and then decreases until a relative stable state is reached. In Fig. 10, the variation of rock mass pressure generally has a similar trend with the convergence of the middle bench (distance changes between Y5 and Y6). Rock mass pressure and convergence increase sharply after middle bench is excavated, and increases slower after lower bench is excavated. After invert arch is excavated, convergence has reached a relative stable state, and rock mass pressure at Y5 and Y6 are still increasing which means that a stable convergence cannot indicate a stable rock mass pressure is reached. This is due to the fact that rheology of rock mass leads to further compaction of rock mass, and it takes longer time compared

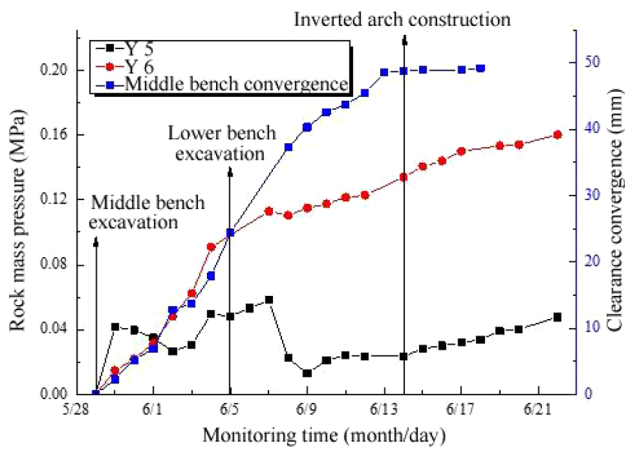


Fig. 10 Sidewall load and middle bench clearance convergence curve

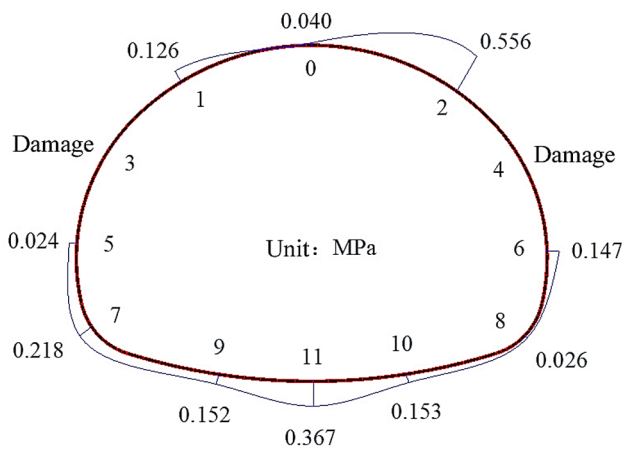
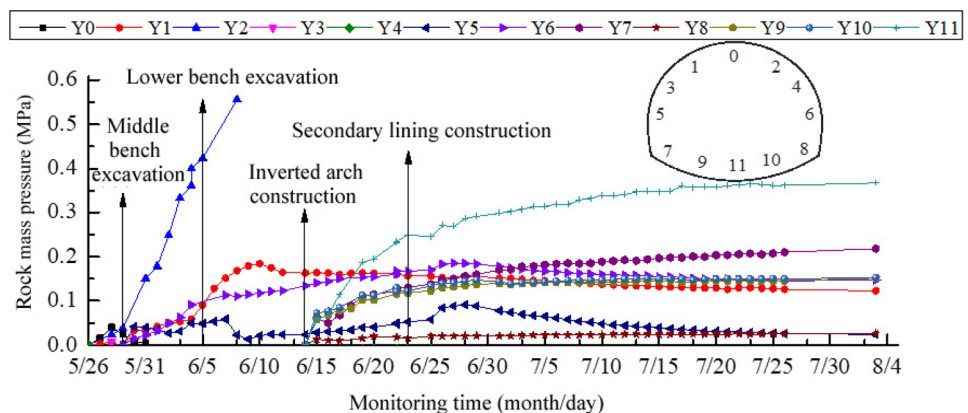


Fig. 11 Rock mass pressure distribution

with that when convergence of the tunnel structure is stable. After the inverted arch was constructed, the rock mass pressure gradually became stable. That was because the tunnel structure reached ring closure, in which the structure forms an oval-like shape.

Fig. 12 Temporal curve of the rock mass pressure in ZK197 + 129 section



Time evolution law of rock mass pressure

The rock mass pressure distribution of ZK197 + 129 section is shown in Fig. 11.

It can be seen from Fig. 10 that: the rock mass pressure is relatively large, and the maximum value is measured at the point 2. It should be noted that the sensor was damaged during measuring, and 0.556 MPa is the maximum effective measured value of the sensor. Generally, the loading is unsymmetrically, and the right side has higher measured rock mass pressure.

The relation between rock mass pressure and construction time is shown in Fig. 12.

To better present the average changing ratio of rock mass pressure, it is calculated at each construction stage at arch (0 to 4 measuring points), sidewall (5 and 6 measuring points), and inverted arch (7 to 11 measuring points). The results are presented in Table 2 and the rock mass pressure ratio is drawn in Fig. 13.

It can be seen from Fig. 12 that the rock mass pressure of arch (Y1 and Y2), increases slowly after the excavation of upper bench, and then increases dramatically after middle bench is excavated. Figure 13a shows that, at point Y1, the rock mass pressure after the excavation of upper bench is 26.83% of final rock mass pressure, the rock mass pressure after the excavation of middle bench is 31.31% of final rock mass pressure, and the rock mass pressure after the excavation of lower bench is 24.22% of final rock mass pressure. It is interesting to note that rock mass pressure increases the most after the excavation of middle bench.

The rock mass pressure of side wall (Y5 and Y6) increases during construction, and Fig. 13b indicated that, point Y6, the rock mass pressure after the excavation of middle bench is 39.81% of final rock mass pressure, and the rock mass pressure after the excavation of lower bench is 32.62% of final rock mass pressure. Together with data from arch section, it is showed that rock mass pressure increases the most after the excavation of middle bench at arch and sidewall. This is due to the fact that middle bench is located

Table 2 Ratio calculation table of rock mass pressure of arch, sidewall and inverted arch

Monitoring part	Construction stage				
	Upper bench excavation	Middle bench excavation	Lower bench excavation	Inverted arch construction (%)	Secondary lining construction (%)
Arch	26.83%	31.31%	24.22%	11.52	6.12
Side wall	–	39.81%	32.62%	17.84	9.73
Inverted arch	–	–	–	68.56	31.44

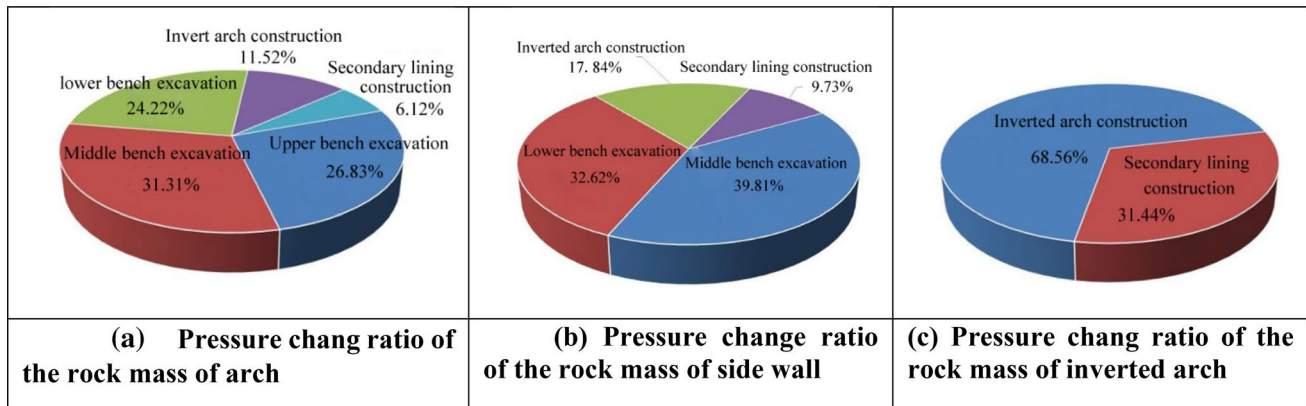


Fig. 13 Pressure change ratio of the rock mass of arch and side wall at each construction stage. **a** Pressure change ratio of the rock mass of arch. **b** Pressure change ratio of the rock mass of side wall. **c** Pressure change ratio of the rock mass of inverted arch

at the maximum excavation line (the maximum width in tunnel section) which is very sensitive to excavation disturbances, and the construction time of middle bench usually takes longer than other parts. It is important to shorten the construction period of middle bench excavation, and provide regular monitoring of stress for safety.

The rock mass pressure of invert (Y7, Y8, Y9, Y10, and Y11) increases dramatically after the construction of invert, and values are stabilized about 35 days after the installation of secondary lining. It lasts about 65–70 days from excavation to final stability. From Fig. 13c, it can be seen that the rock mass pressure after the excavation of invert is 68.56% of final rock mass pressure, and the rock mass pressure after the installation of secondary lining is 31.44% of final rock mass pressure. According to the proportion of rock mass pressure change in each stage, the proportion of rock mass pressure change in the middle bench construction stage is higher than that in the invert construction stage. To decrease the rock mass pressure, ring closure should be reached as soon as possible. It is recommended to speed up the construction of middle bench and lower bench.

The evolution of rock mass pressure with distance to excavation section

The change of rock mass pressure with the distance from the excavation face is shown in Fig. 14. In the figure, D

represents the maximum excavation tunnel diameter which is about 17.0 m. During construction, the excavation speed is about 1.6 m/day.

It can be seen from Fig. 14 that when the monitoring section is within 2D, rock mass pressure is changed rapidly, which is mainly caused by the disturbance of excavation. The rock mass pressure at each part is basically stable when distance is greater than 2.5D (42 m), so the affected distance of tunnel excavation is about 2.5D to the excavation section.

Numerical simulation verification of evolution process of rock mass pressure

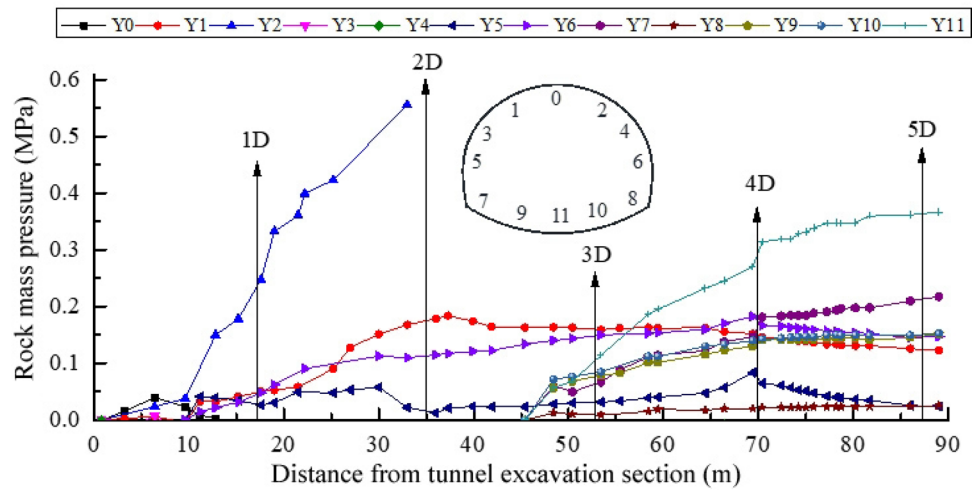
The monitored section is modelled using a three-dimensional finite element model. The evolution of rock mass pressure along with the deformation, construction procedure and distance from the excavation face are analyzed. The simulated law is then compared with the measured results, and the measured results and relations are validated.

The establishment of the model

Assumptions

This simulation makes the following basic assumptions:

Fig. 14 Space curve of the ZK197+129 rock mass pressure



- (1) It is assumed that the rock mass is an elastic-perfectly plastic material which followed the Mohr–Coulomb criterion.
- (2) Initial stress of rock mass only considers gravity stress field and neglects tectonic stress field.
- (3) Reinforcement mesh and longitudinal connection reinforcement rebars in initial supporting are used as safety reserves and are not considered for calculation.
- (4) All materials are isotropic, homogeneous and continuous.
- (5) Supporting structure directly contacts rock mass after installation.

Calculation parameter selection

The mechanical parameters of rock mass used in the numerical calculation are measured by field in-situ tests following the “Guidelines for Design Highway Tunnel” (Ministry of Communications of the People’s Republic of China 2010) and the “Code for Design of Road Tunnel” (Ministry of Communications of the People’s Republic of China 2004). To simplify the model, the steel frame and the shotcrete are simplified as one structure using equivalent conversion method. The conversion calculation is shown in Formulae 1 and 2 (Zhong 2006):

$$E = E_h + \frac{A_g \times E_g}{A_h}, \tag{1}$$

where E Shotcrete elastic modulus after conversion (MPa). Elastic modulus of shotcrete (MPa). A_g Sectional area of steel frame per linear meter (m^2). E_g Elastic modulus of steel frame (MPa). A_h Sectional area of shotcrete per linear meter (m^2).

$$\gamma = \frac{\gamma_{concrete}b + \gamma_{steel}An}{b + An} \tag{2}$$

where γ shotcrete bulk density after conversion (kN/m^3). $\gamma_{concrete}$ shotcrete bulk density (kN/m^3). n number of steel frame in the range of 1 m. A sectional area of steel frame (m^2). b shotcrete thickness (m). γ_{steel} steel frame bulk density (kN/m^3).

Based on “Standard for engineering classification of rock mass” (Ministry of Housing and Urban Rural Development of the People’s Republic of China, General Administration of Quality Supervision, Inspection and Quarantine of the People’s Republic of China, 2014) and “Specifications for Design of Highway Tunnels Section 1 Civil Engineering” (Ministry of Communications of the People’s Republic of China 2018), the parameters and the element types used in this paper are shown in Table 3.

Boundary condition

The distance from tunnel to boundaries is greater than 3.5 time of the tunnel width. The displacement boundary condition of the model is adopted on the both sides, the bottom, the front and back boundaries. In addition, the uniform load is adopted on the top to simulate the buried depth. The model is shown in Fig. 15 and the tunnel detail meshing is shown in Fig. 16.

Analysis of calculation result

Verification of the model

To eliminate the boundary effect in model, the section at $y = 15$ m is selected as the monitoring section in numerical

Table 3 Numerical simulation calculation parameters

	Elastic modulus (MPa)	Poisson’s ratio	Density (kN/m ³)	Cohesion C (kPa)	Internal friction angle(°)	Element types
Rock mass	2200	0.33	26.75	213.4	32.7	Solid element
Initial supporting	28,368.615	0.2	23.31	–	–	Solid element
Feet-lock bolt	210,000	0.3	77	–	–	Beam element
Secondary lining	31,000	0.2	25	–	–	Solid element

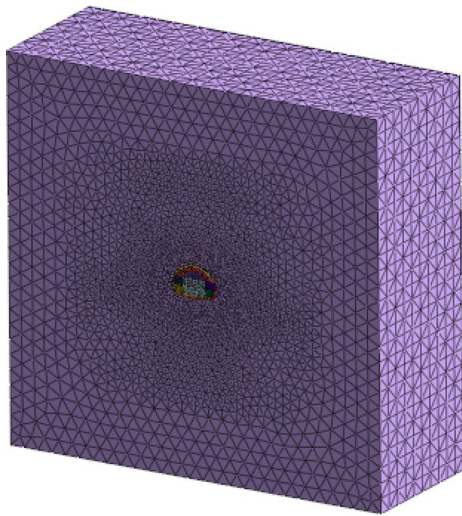


Fig. 15 Schematic of the model

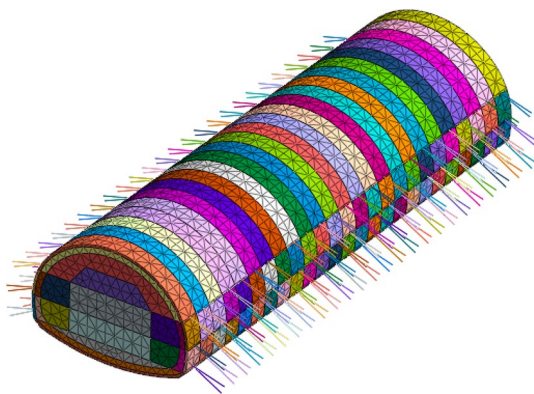


Fig. 16 Meshes considering construction steps

simulation (Wang 2009). The settlement and the clearance convergence nephogram of the tunnel are shown in Figs. 17 and 18.

From Figs. 17 and 18, it can be seen that the crown settlement is about 94.2 mm at the monitoring section and the convergence is about 56.9 mm at the maximum excavation line at the monitoring section. The crown settlement is slightly larger than the measured values which are 85.6 mm.

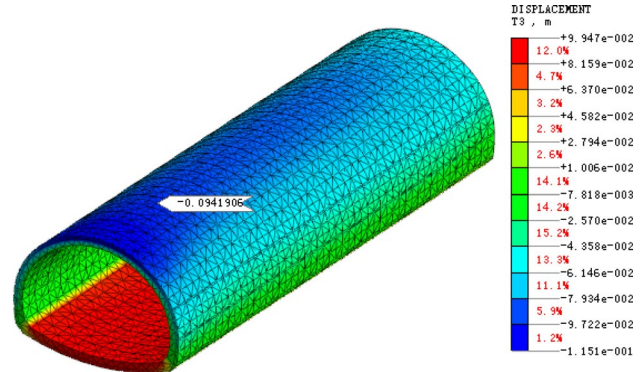


Fig. 17 Nephogram of settlement simulation result

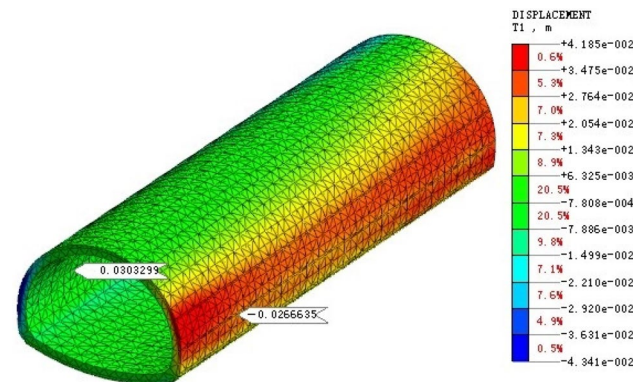


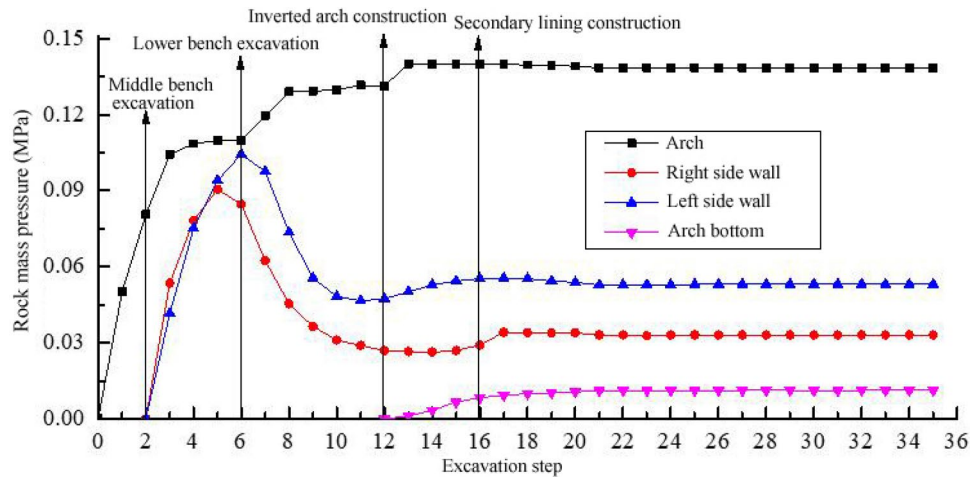
Fig. 18 Nephogram of clearance convergence simulation result

This is due to the fact that in practice it is difficult to monitor initial displacement after construction, so the measured value is slightly smaller than its real value (Luo et al. 2018). In general, the simulation result is basically consistent with the measured values which indicated that parameters are reasonable and the model is valid.

Time evolution law of rock mass pressure

The rock mass pressure at vault, sidewall and arch bottom are extracted. The variation curve of simulation calculation results with the construction steps of rock mass pressure are shown in Fig. 19. The ratio of variation value of rock mass

Fig. 19 Time curve of simulation result of rock mass pressure



pressure to the final stable value at each construction stage is shown in Table 4.

It can be seen from Table 4 and Fig. 19 that: (1) There is little difference between simulated and measured results in the proportion of rock mass pressure variation and the law of rock mass pressure variation with construction procedure, the variation ratio of rock mass pressure in each construction phase and the variation law with the construction process are smaller difference than the measured in Table 3, but the overall law is the same. (2) After the upper bench is excavated, the rock mass pressure growth rate is the fastest, which is due to the larger excavation area and larger disturbance to rock mass. (3) After middle bench is excavated, rock mass pressure at sidewall is increased rapidly, which is due to the excavation of the middle bench generate disturbance and the plastic zone of rock mass is increased rapidly. However, the rock mass pressure of arch increases slightly and then reaches stability. (4) After the inverted arch is constructed, rock mass pressure at arch bottom is increased rapidly and the increasing speed is slowed down at arch part. Due to the inverted arch provides sufficient supporting force for the upper supporting structure, rock mass pressure at sidewall is restored to increase. (5) After the secondary lining is constructed, rock mass pressure quickly reached a stable state. In the measurement, rock mass pressure is not stable

after secondary lining. This is mainly due to the fact that the rheological properties of rock mass are not considered in the numerical calculation.

The spatial evolution law of rock mass pressure

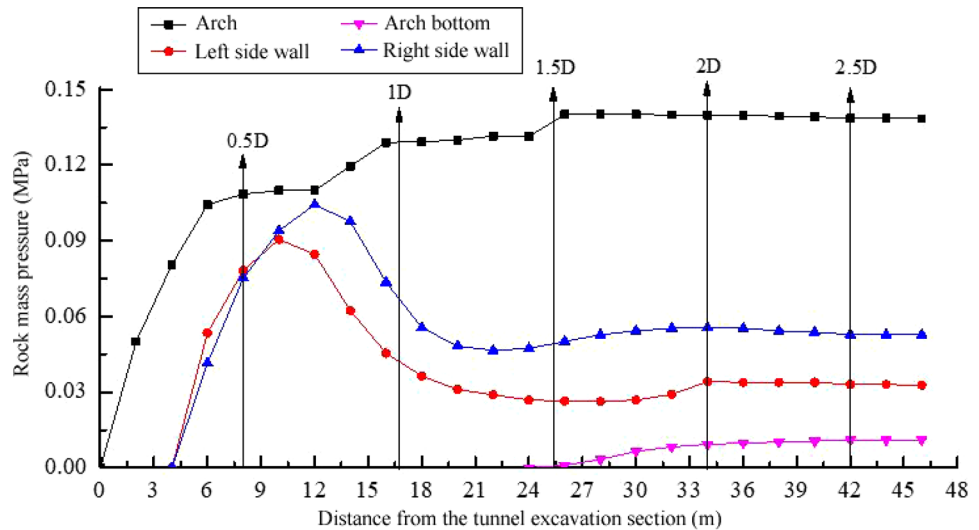
The rock mass pressure is extracted at arch, sidewall and arch bottom. In addition, the curve of distance from the excavation face is shown in Fig. 20.

It can be seen from Fig. 20 that: (1) With the advancement of the excavation face, rock mass pressure of each part is gradually increased. When the distance from the excavation face is 0 to 5 m, the rock mass pressure changes dramatically. (2) Rock mass pressure varies greatly at side wall when the test section is from 5 to 20 m, it is caused by the combined effect of the advancement of the excavation face and transverse effect caused by the excavation of the middle and lower bench of the monitoring section. (3) When the monitored section is more than 30 m away from the excavation section, the rock mass pressure is basically stable and is no longer affected by the excavation of the excavation face. It can be concluded that the space influence of the excavation face is about 2 times to the tunnel diameter (34 m), which is smaller than the measured. This is because the rheology of rock mass is not considered, the rock mass is stable earlier.

Table 4 Simulation results of rock mass pressure at y=15 m section (MPa)

Monitoring positions	Before middle Bench excavation		Before lower Bench excavation		Before Inverted arch apply		Before secondary lining apply		Final stable value
	Rock mass pressure	Ratio	Rock mass pressure	Ratio	Rock mass pressure	Ratio	Rock mass pressure	Ratio (%)	
Vault	0.081	57%	0.110	78%	0.127	90%	0.140	99	0.141
The left side wall	–	–	0.091	276%	0.029	88%	0.027	82	0.033
The right side wall	–	–	0.094	177%	0.047	89%	0.054	102	0.053
Arch bottom	–	–	–	–	–	–	0.008	73	0.011

Fig. 20 Simulation space curve of rock mass pressure



Conclusion

Based on the Lianchengshan tunnel in this paper, the evolution of rock mass pressure of soft-weak rock mass tunnel with deformation, time, space are summarized. The main conclusions are as follows:

- (1) The rock mass pressure experiences about 65 to 70 days to stabilization. After the supporting structure is completed, the variation ratio of rock mass pressure to the final monitored value reaches 70%.
- (2) Before the construction of the middle bench to inverted arch, the changing ratio of rock mass pressure at arch and side wall is extremely high. To decrease the rock mass pressure, ring closure should be reached as soon as possible. It is recommended to speed up the construction of middle bench and lower bench.
- (3) When it is within 1–2 times of the tunnel diameter to the excavation face, the advancement of the excavation face has the greatest influence on rock mass pressure of the excavated part. The space influence range of the excavation face advancement is about 2.5 times of the tunnel diameter (42 m). Beyond this range, the increasing of rock mass pressure is mainly determined by its own rheology, which has little relationship with the propulsion of excavation face.
- (4) By establishing a three-dimensional numerical model, it is found that simulated results are generally consistent with the measured results in terms of rock mass pressure changes. Compared with measured value, the smaller value of rock mass pressure in numerical model is caused by the difficulties of considering all physical properties (rheological property) of rock mass and disturbance during construction and supporting.

Funding Funding was provided by National Key R&D Program of China (Grant No. 2018YFB1600100), National Natural Science Foundation of China (Grant Nos. 51678063, 41831286, 51808049), China Postdoctoral Science Foundation (Grant No. 2016M602738), The Chang Jiang Scholars Program (Grant No. Q2018209) and Natural Science Basic Research Plan of Shaanxi Province (Grant No. 2017JM5051).

References

- Borca T (2002) Investigatory tunnel under way for Lyon-Turin high speed link.
- Chen JX, Liu WW, Chen LJ, Luo YB, Li Y, Gao HJ, Zhong DC (2020) Failure mechanisms and modes of tunnels in monoclinic and soft-hard interbedded rocks: a case study. *KSCE J Civ Eng* 24(4):1–17
- Code for Design of Road Tunnel (JTG D70–2004). People's Communications Publishing House, Beijing.
- Dai YH, Chen WZ, Tian HM, Yang JP, Meng XJ, Deng XL (2015) Study of large deformation and supporting measures of Daliang tunnel with soft rock mass. *Chin J Rock Mech Eng* (s2) 4149–4156
- Galli G, Grimaldi A, Leonardi A (2004) Three-dimensional modelling of tunnel excavation and lining. *Comput Geotech* 31(3):171–183
- Guan BS, Zhao Y (2011) On construction technology in tunnel of soft and weak rock mass. China Communications Press, Beijing, p 216
- Guidelines for design highway tunnel (JTG/T D70–2010). People's Communications Publishing House, Beijing
- Hou Y, Fang Q, Zhang D et al (2015) Excavation failure due to pipeline damage during shallow tunnelling in soft ground. *Tunn Undergr Space Technol* 46(46):76–84
- Hu X, Huang HW (2001) Mechanical analysis of superimposed load introduced by propulsion of adjacent parallel pipe. *Rock Soil Mech* 22(1):75–77
- Hwang JH, Kikumoto M, Kishida K et al (2006) Dynamic stability of multi-arch culvert tunnel using 3-D FEM. *Tunn Undergr Space Technol* 21(3):384

- John DITM (1976) Die geotechnischen Messungen im Arlbergtunnel und deren Auswirkungen auf das Baugeschehen. Springer, Vienna, pp 157–177
- Kimura F, Okabayashi N, Kawamoto T (1987) Tunnelling through squeezing rock in two large fault zones of the Enasan Tunnel II. *Rock Mech Rock Eng* 20(3):151–166
- Kontogianni V, Psimoulis P, Stiros S (2006) What is the contribution of time-dependent deformation in tunnel convergence? *Eng Geol* 82(4):264–267
- Lai JX, Wang KY, Qiu JL et al (2016) Vibration response characteristics of the cross tunnel structure. *Shock Vib* 2016:1–16
- Lai JX, Wang XL, Qiu JL et al (2018) Extreme deformation characteristics and countermeasures for a tunnel in difficult grounds in southern Shaanxi, China. *Environ Earth Sci* 77(19):706
- Lei M, Peng L, Shi C (2015) Model test to investigate the failure mechanisms and lining stress characteristics of shallow buried tunnels under unsymmetrical loading. *Tunn Undergr Space Technol* 46:64–75
- Li D (2012) Study on mechanical properties and optimization method for tunneling of long tunnel through fault zone. Southwest Jiaotong University
- Li DY, Xu ZX, Wang LJ (2007) Numerical simulation analysis of initial supporting system for subway tunnel. *Railw Eng* 5:34–37
- Li LP, Li SC, Zhao Y, Wang HP, Liu Q, Yuan XS, Zhao Y, Zhang Q (2012) Spatial deformation mechanism and load release evolution law of rock mass during construction of super-large section tunnel with soft broken surrounding rock masses. *Chin J Rock Mech Eng* 31(10):2109–2118
- Litwiniszyn J (1956) Application of the equation of stochastic processes to mechanics of loose bodies. *Arch Mech* 8(4):393–411
- Liu C (2007) Study on construction mechanical responses of highway tunnel with deeply-lying and large cross section. Chongqing University
- Liu Q, Li SC, Li LP, Sun KG, Zhao Y (2011) Study of large deformation construction mechanical behavior and supporting measures of soft rock in a deep buried extra long tunnel. *J Shandong Univ (Eng Sci)* 41(3):118–125
- Luo YB, Chen JX, Xi WZ et al (2016) Analysis of tunnel displacement accuracy with total station. *Measurement* 83:29–37
- Luo YB, Chen JX, Xi WZ et al (2017) Application of a total station with RDM to monitor tunnel displacement. *J Perform Constr Facil* 31(4):4017030
- Luo YB, Chen JX, Chen Y et al (2018) Longitudinal deformation profile of a tunnel in weak rock mass by using the back analysis method. *Tunn Undergr Space Technol* 71:478–493
- Meda A, Rinaldi Z, Caratelli A et al (2016) Experimental investigation on precast tunnel segments under TBM thrust action. *Eng Struct* 119:174–185
- Miwa M, Ogasawara M (2005) Tunnelling through an embankment using all ground fasten method. *Tunn Undergr Space Technol* 20(2):121–127
- Ng CW, Lee KM, Tang DK (2004) Three-dimensional numerical investigations of new Austrian tunnelling. *Can Geotech J* 41(3):523–539
- Qiu JL, Liu HQ, Lai JX et al (2018) Investigating the long-term settlement of a tunnel built over improved loessial foundation soil using jet grouting technique. *J Perform Constr Facil* 32(5):04018066
- Shalabi FI (2005) FE analysis of time-dependent behavior of tunneling in squeezing ground using two different creep models. *Tunn Undergr Space Technol* 20(3):271–279
- Shan C (2016) The study of mechanical behavior of highway tunnel going through the existing interurban railway tunnel. Chang'an University
- Specifications for Design of Highway Tunnels Section 1 Civil Engineering (JTG 3370.1–2018). People's Communications Publishing House, Beijing
- Standard for engineering classification of rock mass (GB/T 50218–2014). China Plan Publishing House, Beijing
- Sun YC, Shang YJ (2008) Intergrated analysis of the tempo-spatial effect of surrounding rock deformation in tunneling. *J Eng Geol* 16(2):211–215
- Tang DKW, Lee KM, Ng CWW (2000) Stress paths around a 3-D numerically simulated NATM tunnel in stiff clay. Geotechnical aspects of underground construction in soft ground
- Technical Guidelines for Construction of Highway Tunnel (JTG/TF60–2009). People's Communications Publishing House, Beijing
- Wang HT (2009) Research on mechanism of pipe roof reinforcement and excavation face stability. Dalian University of Technology, Dalian
- Wang M (2014) Study on rock mass mechanical behavior during construction of double tunnel obliquely going through high and steep slope. Southwest Jiaotong University
- Xu QS, Niu YZ, Li QZ (2017) Study on construction mechanics of eccentric tunnel method of double-arch tunnel section of Shenzhen metro line 8. *Highway* 3:256–259
- Yan J, He C, Li DL, Yao ZJ (2017) Analysis of deformation and stress during outwash accumulation tunnel construction. *Railw Stand Des* 61(1):65–71
- Yang SX, Li H, Bai MZ, Xu ZY (2010) The wall-rock's stress releasing regularity arose by cavern excavation in high stress condition. *J China Coal Soc* 01:26–30
- Yang JP, Wang ZY, Li SN, Tang W (2016) Analysis on construction mechanics behavior of soil tunnel considering space-time effect. *J Railw Sci Eng* 13(10):2009–2017
- Yu YX (2004) Study on construction mechanical of the unsymmetrically loading tunnel in geological bedding strata. Southwest Jiaotong University
- Zhao XF, Wang CM, Kong XL (2006) Analysis of time-space effects of construction behavior of deep soft rock tunnel. *J. Rock Mech. Eng.* 26(02):404–409
- Zhao Y, Li SC, Zhao Y, Li LP (2012) Model test study of rock mass load releasing during super-large section tunnel excavation. *Chin J Rock Mech Eng* S2:3821–3830
- Zhong ST (2006) The unified theory of concrete filled steel tube. Tsinghua University Press, Beijing, pp 21–27
- Zou C, Wang CP, Zhang WX, Gao P (2010) Experimental study on stress control in carbonaceous slate section of Muzhailing tunnel on Lanzhou-Chongqing railway. *Tunn Constr* 30(2):120–124
- Zuo QJ, Chen K, Tan YZ, Hu SS, Wang HX (2016) A time-dependent constitutive model of the water-rich argillaceous slate surrounding a tunnel. *Rock Soil Mech* 37(5):1357–1364

Publisher's Note Springer Nature remains neutral with regard to jurisdictional claims in published maps and institutional affiliations.